INTERNATIONAL JOURNAL FOR NUMERICAL METHODS IN FLUIDS, VOL. 22, 1189–1205 (1996)

OPERATOR-SPLITTING COMPUTATION OF TURBULENT FLOW IN AN AXISYMMETRIC 180° NARROWING BEND USING SEVERAL k–ε MODELS AND WALL FUNCTIONS

X.-L. LUO

CSIRO Division of Mathematics and Statistics, Locked Bag 17, North Ryde, N.S.W. 2113, Australia

SUMMARY

This paper describes a finite element implementation of an operator-splitting algorithm for solving transient/steady turbulent flows and presents solutions for the turbulent flow in an axisymmetric 180° narrowing bend, a benchmark problem dealt with at the 1994 WUA-CFD annual meeting. Three k–ε based models are used: the standard linear k–ε model, a non-linear k–ε model and an RNG k–ε model.

Flow separation after the bend, as observed in the experiment, is predicted by the RNG model and by both the linear and non-linear k–ε models with van Driest mixing length wall functions. Good agreement with experimental data of pressure distribution on bending walls is obtained by the present numerical simulation. Results show that there is very little difference between the linear and non-linear k–ε models in terms of predicted velocity fields and that the non-linearities mainly affect the distribution of turbulent normal stress and pressure, in analogy to the effect of second-order viscoelastic fluid models on laminar flow. Both the linear and non-linear k–ε models fail to predict any flow separation if logarithmic wall functions are used.

KEY WORDS: turbulence model; finite element; flow separation; operator splitting; axisymmetric bend

1. INTRODUCTION

In the last decade or so, the impact of the finite element method (FEM) upon the numerical modelling of turbulent flows of industrial complexity, a field traditionally dominated by finite difference/finite volume techniques, has been increasing steadily.[1] Overcoming some of the earlier difficulties associated with applying the FEM to turbulent flow, a large range of turbulent flow problems have been solved successfully by a variety of finite element approaches.[2–10]

Since the original version of the k–ε model was developed by Launder and co-workers in 1972,[12,13] it has been most widely used by engineers and scientists for the solution of practical problems. A variety of modified versions have been proposed to improve the performance of the model, among which are the renormalization group (RNG)-based models[16–19] and the non-linear k–ε models.[20,21] The RNG method describes the complex dynamics of turbulence in terms of so-called 'coarse-grained' equations of motion governing the large-scale, long-time behaviour of the physical system; it gives a theory of the Kolmogorov equilibrium range of turbulence, especially the inertial range of small-scale eddies. The latest version of the RNG model proposed by Yakhot and co-workers,[18,19] which incorporates a modification of the production-of-dissipation term to account for non-equilibrium strain rates will be used in the present study.

CCC 0271–2091/96/121189–17

Received 28 October 1994
Revised 9 October 1995

The non-linear k–ε model proposed by Speziale[21] has a structure similar to that of a Rivlin–Ericksen fluid, which is a second-order viscoelastic model and is used to describe flows of dilute polymer solutions.[22,23] This non-linear k–ε model overcomes the inability of the standard k–ε model and all its linear variations to predict normal stress difference, which is a common feature of Newtonian turbulent shear flow and non-Newtonian laminar shear flow. The inability of the linear k–ε model to predict normal stress difference makes it impossible to describe effects such as secondary flows in non-circular ducts.[24] The non-linear k–ε model was subsequently applied to the backward-facing step problem, yielding better results than those of the linear k–ε model.[25,26]

One of the benchmark problems at the 1994 annual meeting of the World User Association in Applied Computational Fluid Dynamics (WUA-CFD '94) was the turbulent flow in an axisymmetric 180° narrowing bend ('bend problem' for short). A schematic diagram of the basic geometry and flow field is shown in Figure 1 (see Section 4). Although there are no sharp corners in the geometry, the bend problem appears to be more difficult than the flow over a backward-facing step. One major question is whether the flow separation after the bend, as observed in the experiment, can be predicted by a k–ε model. In the backward-facing step problem, numerical modelling can always predict a recirculation behind the step and the concern there is only how large the recirculation should be. The sharp step and high flow inertia 'force' the initial formation of recirculation and the detachment point is fixed at the step corner. In the bend problem, however, a balance among pressure, inertia, viscous and turbulent stresses will determine whether there is a flow separation and the position of the detachment point is unknown if there is a flow separation. A high pressure gradient normal to the bending wall makes some universal wall functions totally unsuitable in that region.

Does the standard k–ε model predict separation for the bend problem? The answers to this important question from some of the well-known commercial CFD codes presented at WUA-CFD '94 are mixed.[27–29] FLUENT and FLOW3D concluded that the standard k–ε model predicted no separation, while FIDAP did predict separation with the standard k–ε model. Both FLUENT and FLOW3D predicted flow separation with an RNG-based k–ε model.

Another question to ask is how the RNG model and the non-linear k–ε model would perform in the bend problem in comparison with the standard k–ε model and with experimental data. This question can only be partially answered here, since there are insufficient experimental data such as turbulent stress field available for a detailed comparison. However, a comparison of this kind still reveals some interesting aspects of these three models.

2. GOVERNING EQUATIONS

For the turbulent flow of an incompressible viscous fluid the Reynolds-averaged Navier–Stokes equation and continuity equation are given by

$$\rho \frac{\partial \mathbf{u}}{\partial t} + \rho(\mathbf{u} \cdot \nabla)\mathbf{u} + \nabla p - \mu \nabla^2 \mathbf{u} = \nabla \cdot \boldsymbol{\tau}, \tag{1}$$

$$\nabla \cdot \mathbf{u} = 0, \tag{2}$$

where ρ is the fluid density, $\mathbf{u}$ is the mean velocity, p is the mean pressure, μ is the dynamic viscosity of the fluid and $\boldsymbol{\tau}$ is the Reynolds stress tensor whose components are given by

$$\tau_{ij} = -\rho \overline{v_i v_j}, \tag{3}$$

where $\mathbf{v}$ is the fluctuation part of the velocity.

For achieving closure, equations relating the Reynolds stress tensor to the global history of the mean velocity field are needed. For the k–ε based model of turbulence the Reynolds stress tensor is expressed as a tensor function of mean velocity $\mathbf{u}$, turbulent kinetic energy k and turbulence dissipation rate ε.

2.1. *Standard linear k–ε model*

The standard linear k–ε model[12,13] is of the form

$$\tau_{ij} = -\tfrac{2}{3}\rho k\delta_{ij} + 2\mu_t D_{ij}, \tag{4}$$

where

$$k = -\frac{1}{2\rho}\tau_{ii}, \tag{5}$$

$$\mu_t = \rho C_\mu \frac{k^2}{\varepsilon}, \tag{6}$$

$$D_{ij} = \frac{1}{2}\left(\frac{\partial u_i}{\partial x_j} + \frac{\partial u_j}{\partial x_i}\right) \tag{7}$$

are the turbulent kinetic energy, turbulent viscosity and mean rate-of-strain tensor respectively. For an incompressible flow the δ_{ij}-term in (4) is pressure-like and makes no contribution to turbulence generation.

The transport equations for k and ε at high Reynolds numbers are given by

$$\frac{\partial k}{\partial t} + (\mathbf{u}\cdot\nabla)k - \nabla\cdot\left[\left(\nu_0 + \frac{\nu_t}{\sigma_k}\right)\nabla k\right] + \varepsilon = G, \tag{8}$$

$$\frac{\partial \varepsilon}{\partial t} + (\mathbf{u}\cdot\nabla)\varepsilon - \nabla\cdot\left[\left(\nu_0 + \frac{\nu_t}{\sigma_\varepsilon}\right)\nabla\varepsilon\right] + C_2\frac{\varepsilon^2}{k} = C_1\frac{\varepsilon}{k}G, \tag{9}$$

where $\nu_0 = \mu/\rho$ and $\nu_t = \mu_t/\rho$ are the kinetic viscosities and G is the turbulent generation term

$$G = \nu_t\left(\frac{\partial u_i}{\partial x_j} + \frac{\partial u_j}{\partial x_i}\right)\frac{\partial u_i}{\partial x_j}. \tag{10}$$

The five constants have the following commonly used values:

C_μ	C_1	C_2	σ_k	σ_ε
0·09	1·44	1·92	1·0	1·30

In general the k–ε model is only valid in fully turbulent regions. Close to a solid wall, viscous effects become dominant and a special treatment is required in order to obtain realistic numerical predictions. In this study the simple but efficient effective viscosity wall function approach will be taken. Two different sets of wall functions will be used here. The following single-layer log-wall model has been widely used in control-volume-based CFD codes:[25,30–32]

$$y^+ = \rho\delta C_\mu^{0\cdot25}k^{0\cdot5}/\mu, \tag{11}$$

$$\mu_t = 0\cdot0 \quad \text{if } y^+ < 11\cdot5, \tag{12}$$

$$\mu_t = \rho\kappa C_\mu^{0\cdot25}k^{0\cdot5}\delta/\ln(Ey^+) \quad \text{if } y^+ > 11\cdot5, \tag{13}$$

where δ is the normal distance to the wall, $E = 9{\cdot}79$ and $\kappa = 0{\cdot}419$ for smooth walls.[31] The above one-layer lon-wall model will be denoted as WF1 for convenience. WF1 essentially specifies an effective viscosity derived from a logarithmic velocity profile.

Also adopted in this study is the van Driest[11] mixing length approach, which will be denoted as WF2, in which the turbulent viscosity in the equilibrium wall layer is modelled as

$$\mu_t = \rho l_m^2 \left[\left(\frac{\partial u_i}{\partial x_j} + \frac{\partial u_j}{\partial x_i} \right) \frac{\partial u_i}{\partial x_j} \right]^{1/2}, \tag{14}$$

where l_m is the mixing length. For smooth walls, l_m is obtained from van Driest's equation

$$l_m = \kappa\delta[1 - \exp(-y^+/A)], \tag{15}$$

in which A is an empirical constant assuming the value of 26 for smooth walls. The exponential damping function in the van Driest mixing length progressively suppresses the mixing length as y^+ diminishes.

The wall functions are applied within the special wall layer elements, with the k–ε equations being solved only in the region excluding the viscous sublayer.

2.2. *Non-linear k–ε model*

The non-linear k–ε model of Speziale[21] can be described as

$$\tau_{ij} = -\tfrac{2}{3}\rho k\delta_{ij} + \rho k^{1/2} l_t D_{ij} + 4C_D \rho l_t^2 (D_{im}D_{mj} - \tfrac{1}{3}D_{mn}D_{mn}\delta_{ij}) + 4C_E \rho l_t^2 (\hat{D}_{ij} - \tfrac{1}{3}\hat{D}_{mm}\delta_{ij}), \tag{16}$$

where

$$l_t = C_\mu \frac{K^{3/2}}{\varepsilon}, \tag{17}$$

D_{ij} is the strain rate tensor and $\hat{D}_{ij}$ is its Oldroyd derivative

$$\hat{D}_{ij} = \frac{\partial D_{ij}}{\partial t} + \mathbf{u}\cdot\nabla D_{ij} - \frac{\partial u_i}{\partial x_k} D_{kj} - \frac{\partial u_j}{\partial x_k} D_{ki}. \tag{18}$$

The two extra constants $C_D = C_E = 1{\cdot}68$. The transport equations for k and ε are the same as the linear model, except that the generation term expressed in (10) has to be replaced by a more general form of the product of stress and strain rate,

$$G = \tau_{ij} \left(\frac{\partial u_i}{\partial x_j} + \frac{\partial u_j}{\partial x_i} \right) \Big/ \rho, \tag{19}$$

where τ_{ij} is given by (16). Again all the δ_{ij}-terms in τ_{ij} are pressure-like and make no contribution to the generation of k and ε in an incompressible flow.

Care must be taken to include correctly the extram terms involving u/r for τ_{ij} in an axisymmetric flow. The axisymmetric component form of the Oldroyd derivative is given by

$$\hat{D}_{zz} = \frac{\partial D_{zz}}{\partial t} + u_z \frac{\partial D_{zz}}{\partial z} + u_r \frac{\partial D_{zz}}{\partial r} - 2\left(\frac{\partial u_z}{\partial z}\right)^2 - \left(\frac{\partial u_z}{\partial r} + \frac{\partial u_r}{\partial z}\right)\frac{\partial u_z}{\partial r}, \tag{20}$$

$$\hat{D}_{rr} = \frac{\partial D_{rr}}{\partial t} + u_z \frac{\partial D_{rr}}{\partial z} + u_r \frac{\partial D_{rr}}{\partial r} - 2\left(\frac{\partial u_r}{\partial r}\right)^2 - \left(\frac{\partial u_z}{\partial r} + \frac{\partial u_r}{\partial z}\right)\frac{\partial u_r}{\partial z}, \tag{21}$$

$$\hat{D}_{rz} = \frac{\partial D_{rz}}{\partial t} + u_z \frac{\partial D_{rz}}{\partial z} + u_r \frac{\partial D_{rz}}{\partial r} - \frac{\partial u_z}{\partial r}\frac{\partial u_r}{\partial r} - \frac{\partial u_r}{\partial z}\frac{\partial u_z}{\partial z} + \frac{u_r}{r}\left(\frac{\partial u_z}{\partial r} + \frac{\partial u_r}{\partial z}\right)\Big/2, \tag{22}$$

$$\hat{D}_{\theta\theta} = \frac{\partial D_{\theta\theta}}{\partial t} + u_z \frac{\partial D_{\theta\theta}}{\partial z} + u_r \frac{\partial D_{\theta\theta}}{\partial r} - 2\left(\frac{u_r}{r}\right)^2, \tag{23}$$

from which the components of the non-linear turbulent stress tensor can be readily worked out.

The presence of the Oldroyd derivative makes the non-linear k–ε model bears a certain resemblance to the Rivlin–Ericksen fluids of viscoelastic flow and we will see some similar effects on the velocity and pressure fields. Like its linear counterpart, the non-linear k–ε model also needs wall functions in near-wall regions.

2.3. *RNG k–ε model*

Yakhot and co-workers have recently proposed the RNG-based k–ε model[17,19]

$$\nu_t = \nu_0\left[1 + \left(\frac{C_\mu}{\nu_0}\right)^{1/2}\frac{k}{\varepsilon^{1/2}}\right]^2, \tag{24}$$

$$\frac{\partial k}{\partial t} + (\mathbf{u}\cdot\nabla)k - \nabla\cdot\left[\left(\nu_0 + \frac{\nu_t}{\sigma_k}\right)\nabla k\right] + \varepsilon = G, \tag{25}$$

$$\frac{\partial \varepsilon}{\partial t} + (\mathbf{u}\cdot\nabla)\varepsilon - \nabla\cdot\left[\left(\nu_0 + \frac{\nu_t}{\sigma_\varepsilon}\right)\nabla\varepsilon\right] + C_2\frac{\varepsilon^2}{k} + R = C_1\frac{\varepsilon}{k}G, \tag{26}$$

where R is an extra strain rate term given by

$$R = \frac{C_\mu\eta^3(1-\eta/\eta_0)\varepsilon^2}{(1+\beta_0\eta^3)k}, \tag{27}$$

with

$$\eta = \frac{k}{\varepsilon}\left[\left(\frac{\partial u_i}{\partial x_j} + \frac{\partial u_j}{\partial x_i}\right)\frac{\partial u_i}{\partial x_j}\right]^{0.5} \tag{28}$$

The constants used for the new RNG model are as follows:

C_μ	C_1	C_2	σ_k	σ_ε	β_0	η_0
0·0845	1·42	1·68	0·7179	0·7179	0·012	4·38

The total turbulent stress has the same expression as the linear k–ε model given by (4). Comparing with the linear k–ε model, this RNG model has different constant values and an extra strain rate term in the ε-equation. It also has a single turbulent viscosity expression which is valid across the full range of flow conditions from low to high Reynolds numbers.[19]

3. NUMERICAL ALGORITHM

3.1. *Operator splitting*

The operator-splitting method treats non-linearity and incompressibility in the Navier–Stokes equations separately at different fractional time steps.[33–36] The method is suitable for both steady and transient problems and can readily be extended to include extra equations describing additional physical effects such as heat transfer and turbulence.

The following segregated time-stepping scheme is used to solve the coupled non-linear system of the k–ε turbulence model.

(1) Solve for k^{n+1} and ε^{n+1} by a semi-implicit method using a GMRES iterative solver:

$$\frac{k^{n+1}-k^n}{\Delta t}+0{\cdot}5(\mathbf{u}^n\cdot\nabla)(k^{n+1}+K^n)-0{\cdot}5\nabla\cdot\left[\left(\nu_0+\frac{\nu_t^n}{\sigma_k}\right)\nabla(k^{n+1}+k^n)\right]=-\varepsilon^n+G^n, \quad (29)$$

$$\frac{\varepsilon^{n+1}-\varepsilon^n}{\Delta t}+0{\cdot}5(\mathbf{u}^n\cdot\nabla)(\varepsilon^{n+1}+\varepsilon^n)-0{\cdot}5\nabla\cdot\left[\left(\nu_0+\frac{\nu_t^n}{\sigma_\varepsilon}\right)\nabla(\varepsilon^{n+1}+\varepsilon^n)\right]+C_2\frac{\varepsilon^n}{k^n}\varepsilon^{n+1}=C_1\frac{\varepsilon^n}{k^n}G^n. \quad (30)$$

Similar algorithms can be used for the non-linear and RNG k–ε models.

(2) Update the turbulent viscosity ν_t^{n+1} and extra turbulent stresses in the case of the non-linear k–ε model. Since the δ_{ij}-term can be absorbed in the pressure for incompressible flow, the linear and RNG k–ε models can be treated purely as variable viscosity models and the pressure-like term needs to be computed only when recovering the real pressure. We define the extra turbulent stress S_{ij} for the non-linear k–ε model as the difference between the total stress and the linear model contribution,

$$S_{ij}=\tau_{ij}-(-\tfrac{2}{3}\rho k\delta_{ij}+2\mu_t D_{ij})=4C_D\rho l_t^2(D_{im}D_{mj}-\tfrac{1}{3}D_{mn}D_{mn}\delta_{ij})+4C_D\rho l_t^2(\hat{D}_{ij}-\tfrac{1}{3}\hat{D}_{mm}\delta_{ij}), \quad (31)$$

which is explicitly computed at every time step for the non-linear model.

(3) Solve for $\mathbf{u}^{n+1}$ and p^{n+1} the Reynolds-averaged momentum equations by operator splitting in three fractional steps:[33–36]

first fractional step

$$\frac{\mathbf{u}^{n+\theta}-\mathbf{u}^n}{\theta\Delta t}-\alpha\nabla\cdot(\nu^n\nabla\mathbf{u}^{n+\theta})+\nabla p^{n+\theta}=\beta\nabla\cdot(\nu^n\nabla\mathbf{u}^n)-(\mathbf{u}^n\cdot\nabla)\mathbf{u}^n+\nabla\cdot[\nu^n(\nabla\mathbf{u}^n)^{\mathrm{T}}]+\nabla\cdot\mathbf{S}^n, \quad (32)$$

$$\nabla\cdot u^{n+\theta}=0, \quad (33)$$

second fractional step

$$\frac{\mathbf{u}^{n+1-\theta} - \mathbf{u}^{n+\theta}}{(1-2\theta)\Delta t} - \beta\nabla\cdot(\nu^n\nabla\mathbf{u}^{n+1-\theta}) + (\mathbf{u}^{n+1-\theta}\cdot\nabla)\mathbf{u}^{n+1-\theta} + \nabla\cdot[\nu^n(\nabla\mathbf{u}^{n+1-\theta})^{\mathrm{T}}]$$

$$= \alpha\nabla\cdot(\nu^n\nabla\mathbf{u}^{n+\theta}) - \nabla p^{n+\theta} + \nabla\cdot\mathbf{S}^n, \tag{34}$$

third fractional step

$$\frac{\mathbf{u}^{n+1} - \mathbf{u}^{n+1-\theta}}{\theta\Delta t} - \alpha\nabla\cdot(\nu^n\nabla\mathbf{u}^{n+1}) + \nabla p^{n+1}$$

$$= \beta\nabla\cdot(\nu^n\nabla\mathbf{u}^{n+1-\theta}) - (\mathbf{u}^{n+1-\theta}\cdot\nabla)\mathbf{u}^{n+1-\theta} + \nabla\cdot[\nu^n(\nabla\mathbf{u}^{n+1-\theta})^{\mathrm{T}}] + \nabla\cdot\mathbf{S}^n, \tag{35}$$

$$\nabla\cdot\mathbf{u}^{n+1} = 0, \tag{36}$$

where $\nu^n = \nu_0 + \nu_t^n$ is the total viscosity at the nth time step. The extra stress term $\nabla\cdot\mathbf{S}^n$ is only for the non-linear k–ε model.

The subproblems at the first and third fractional steps are identical and are of the type of steady Stokes problem with variable viscosity:

$$\alpha_1\mathbf{u} - \nabla\cdot(\nu_1\nabla\mathbf{u}) + \theta\nabla p = \mathbf{F}_1, \tag{37}$$

$$\nabla\cdot\mathbf{u} = 0, \tag{38}$$

with $\alpha_1 = 1/\Delta t$ and $\nu_1 = \alpha\theta\nu$.

The subproblem at the second fractional step is of the type of classical non-linear diffusion–convection problem:

$$\alpha_1\mathbf{u} - \nabla\cdot(\nu_2\nabla\mathbf{u}) + (1-2\theta)(\mathbf{u}\cdot\nabla)\mathbf{u} = \mathbf{F}_2, \tag{39}$$

with $\nu_2 = \beta(1-2\theta)\nu$.

In the above scheme, $\alpha, \beta \in (0, 1)$, $\alpha + \beta = 1$ and $\theta \in (0, \frac{1}{3})$. A good choice for θ was found[34,35] to be $1 - 1/\sqrt{2}$. The value of α and β are chosen in such a way that $\nu_1 = \nu_2$ is satisfied to yield identical Helmholtz operators at all fractional steps, which contributes considerably to the overall efficiency of the operator-splitting algorithm.

The Stokes problem is solved by a preconditioned conjugate gradient method. The non-linear diffusion–convection problem is first reformulated as a least squares problem and then solved by a preconditioned conjugate gradient method. This scheme reduces the solution of the Navier–Stokes equations to solving a sequence of scalar Dirichlet problems associated with the Helmholtz operator and the Neumann problems associated with the Laplacian operator. The matrix associated with the Helmholtz operator is well conditioned for all Reynolds numbers, since $\alpha_1 = 1/\Delta t$. More details on the algorithm of operator splitting and preconditioned conjugate gradient iterations are given by Glowinski and co-workers.[33–36]

3.2. Finite element implementation

The variational form of the above numerical system is discretized with Galerkin finite element procedures. Eight-node quadrilateral elements are used for velocity, k and ε; four-node linear elements are used for pressure. Integration by parts (IBP) is done for all the diffusion terms. IBP on the extra stress divergence terms for the non-linear k–ε model results in extra boundary integrations for the momentum equation, which have to be explicitly computed on boundaries where stress-type conditions are imposed.

The entire code is expressed in a special high-level language called *Fasttalk*, which is a unique feature of *Fastflo*,[37] a general-purpose finite element CFD package under development at the CSIRO Division of Mathematics and Statistics in Australia. *Fastflo* contains no physical assumptions nor mathematical algorithms; it purely supports *Fasttalk* language, assemblies and solves finite element equations as programmed by *Fasttalk*. Resembling a general partial differential equation solution environment, *Fastflo* also provides facilities for special applications such as turbulence modelling. For example, the turbulent generation term G can be conveniently computed using *Fasttalk*'s special provisions. Interested readers can find more information on *Fastflo* and *Fasttalk* in Reference 37, where a World Wide Web site has also been given.

4. RESULTS AND DISCUSSION

4.1. Geometry and boundary conditions

A schematic diagram of the flow field is shown in Figure 1. The geometry contains a circular inlet section with radius $R_1 = 4{\cdot}5$ cm, followed by a narrowing 180° bend and an annular outlet with gap $R_2 = 1{\cdot}88$ cm. The gap between inlet and outlet is $D_1 = 1{\cdot}22$ cm. The broken line in Figure 1 is the axis of symmetry and the thick full lines represent solid walls. The narrowing bend can be described by the internal and external boundary bending curves. The internal bending curve is a perfect semicircle with diameter D_1. The external bending curve is quite complicated; it consists of several piecewise arcs specified by about 18 length and angle parameters. Exact details of the geometry can be found in the WUA-CFD Test Case 1/93 description sheet.[38] Figure 2 shows the finite element mesh used in the calculations.

The Reynolds number based on inlet uniform velocity u_{in} is

$$Re = \rho u_{in} D_{in}/\mu = 286{,}000. \tag{40}$$

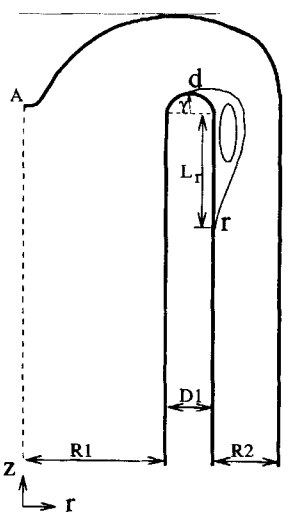

Figure 1. Schematic diagram of turbulent flow in an axixymmetric narrowing bend

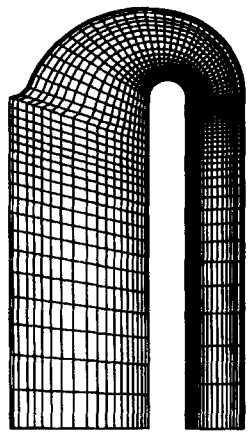

Figure 2. Finite element mesh for the bend problem, with 5054 nodes

In dimensionless form we let $u_{in} = 1$, inlet pipe diameter $D_{in} = 2R_1 = 9$, fluid density $\rho = 1$ and viscosity $\mu = 3{\cdot}146853 \times 10^{-5}$ to obtain the correct Reynolds number. The inflow boundary conditions for k and ε represent a turbulent intensity I_t of 10%:

$$k_{in} = \tfrac{3}{2}(u_{in}I_t)^2, \qquad \varepsilon_{in} = \frac{(0{\cdot}09)^{0{\cdot}75}(k_{in})^{1{\cdot}5}}{0{\cdot}07(D/2)}. \tag{41}$$

A range of values of k_{in} and ε_{in} have been used in the literature and for most modelling applications the predictions have been found to be insensitive to these values. The outflow has a normal stress boundary condition, assuming a fully developed outflow. The contribution to the boundary integration by the non-zero normal stress of the non-linear k–ε model has to be explicitly computed.

On solid walls, a no-slip velocity BC applies. The solution domain for k and ε excludes the wall layer elements and boundary conditions for k and ε are imposed on top of the 'inner' domain. A Neumann boundary condition on k and a Dirichlet boundary condition on ε are imposed:

$$\frac{\partial k}{\partial n} = 0, \qquad \varepsilon = \frac{C_\mu^{0{\cdot}75}k^{1{\cdot}5}}{\kappa\delta}. \tag{42}$$

On the outlet boundary we have

$$\frac{\partial k}{\partial n} = 0, \qquad \frac{\partial \varepsilon}{\partial n} = 0. \tag{43}$$

Over the entire domain the initial conditions are zero for velocity and pressure and the inlet values for k and ε. The initial turbulent viscosity is computed from the initial values of k and ε. The RNG model uses a single viscosity functions throughout the entire region without any *ad hoc* wall damping functions.

4.2. Solution strategy and convergence

The segregated time-stepping scheme described in Section 3 was carried out for all three models. The time step value Δt was automatically adjusted according to the convergence performance of the preconditioned conjugate gradient (PCG) iterations in operator splitting for the N–S equations. If the number of iterations taken by PCG in one of the fractional steps exceeded 20, the time step was automatically reduced by half, and if the number of iterations was less than 10, the time step was

increased by 20%. The time step was also reduced by half if the time derivative of velocity increased from the previous time step, i.e. if the ratio of time derivatives in the last two consecutive time steps exceeded unity. This seemed to work very well in balancing between stability and efficiency of the time-stepping runs. The initial time step was set to 0·01 dimensionless time unit. Steady state was considered to be reached when all the relative time derivatives of velocity, pressure, k and ε satisfied

$$\Theta \equiv \frac{|v^{n+1} - v^n|}{\Delta t |v^{n+1}|} < 10^{-3}, \tag{44}$$

where v^{n+1} and v^n represent solutions for any one of the above-mentioned variables at two consecutive time steps. The norm $|v|$ is defined as

$$|v| = \sqrt{\left(\sum_i v_i^2\right)}, \tag{45}$$

in which v_i denotes the ith node point value.

It was found that except for some isolated time steps the time derivative Θ monotonically decreased from $1/\Delta t = 100$ at the first time step to below 10^{-3} when steady state was reached. Consistent with this stable time stepping, the automatically adjusted time step value increased monotonically. However, in order to minimize or even eliminate the effect of possible negative values of k and ε, we found it necessary to limit the maximum time step value, since the number of negative points and the magnitude of negative values seemed to be in proportion to the magnitude of time steps. In this study we found it satisfactory to limit the maximum time step value at 0·1. Nodal value clipping was still necessary when some isolated negative values of k or ε (very small in magnitude owintg to small time steps) occurred in the solutions.

Since the time step value was 0·1 when reaching steady state, the criterion specified in (44) corresponds to the relative change in solution being less than 10^{-4}. The entire solution strategy described above was carried out automatically by the *Fasttalk* code; no user interference was necessary.

SUPG-type upwinding was applied to the k- and ε-equations and the momentum equation. The convergence criterion for the GMRES iterative solver used for the k- and ε-equations was to let the preconditioned residual be less than 10^{-7}.

4.3. Calculations with WF1

The logarithmic effective viscosity wall function (WF1) was first used for both the standard linear and non-linear k–ε models. The calculations predicted no separation. This is the same conclusion reached in several reports at WUA-CFD '94, including FLOW3D and FLUENT.[27,28,39] On the other hand, several other reports, including FIDAP's, at the same meeting concluded that the standard k–ε model does predict flow separation for this problem.[29,40] We will discuss more about this controversy after the next subsection.

4.4. Calculations with WF2

Using the van Driest mixing length wall function (WF2), calculations for both the linear and non-linear k–ε models predicted flow separation without any difficulty. Figures 3 and 4 show contours of the solutions for the linear and non-linear k–ε models respectively.

Now it is clear that whether the standard k–ε model can predict flow separation in this benchmark problem depends on what wall functions are used, since the only difference in our calculations with WF1 and WF2 was in the wall functions. This was also evident from two reports[29,39] at WUA-CFD '94 which actually stated what kinds of wall functions were used. One used logarithmic wall functions and

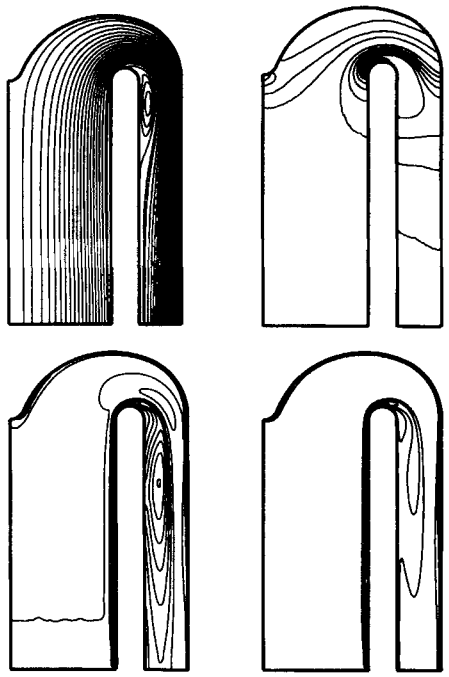

Figure 3. Contour plots for linear k–ε model with WF2. Clockwise from top left: streamline, pressure, ε and k

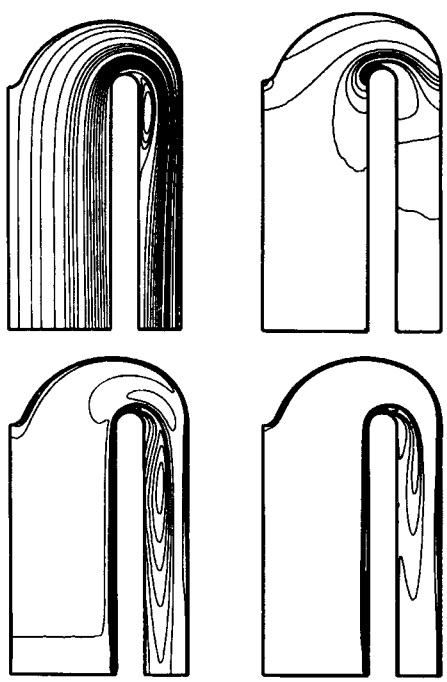

Figure 4. Contour plots for non-linear k–ε model. Clockwise from top left: streamline, pressure, ε and k

failed to predict flow separation;[39] the other used essentially the same wall functions as WF2 used here and predicted flow separation.[10,29] It is not known to the author what kinds of wall functions were used in the other studies presented at WUA-CFD '94.

The complete failure of WF1 to predict flow separation is probably due to its complete inadequacy in regions where there is a large pressure gradient normal to the wall and the logarithmic velocity profile assumption is totally invalid there. On the other hand, the van Driest mixing length approach does not necessarily impose a logarithmic velocity profile in the near-wall region.

Since the initial conditions for all variables are artificially imposed, they did not represent a true physical state of the flow (e.g. zero velocity with non-zero k and ε), which, we found, caused a severe instability in the non-linear k–ε model at early time steps: the time derivative term in the Oldroyd derivative $\partial D_{ij}/\partial t$ contributed to a strong negative generation of k and ε at early time steps. This transient term was then omitted, since we were only interested in the final steady state solution, and the calculation became stable without this term.

4.5. Calculations with RNG model

The RNG model also predicted flow separation without any difficulty. Figure 5 shows contour plots of the RNG model solutions. In fact, all RNG-based calculations reported at WUA-CFD '94 predicted flow separation. Like the van Driest mixing length treatment, the RNG model does not impose a logarithmic velocity profile in near-wall regions, since it uses a single viscosity function throughout the entire region.

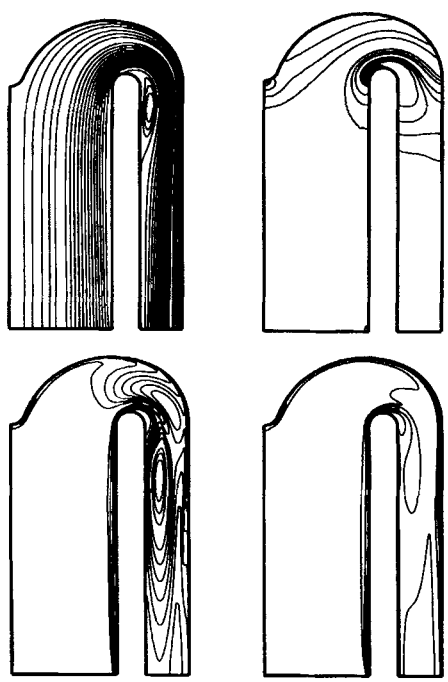

Figure 5. Contour polts of RNG k–ε model solutions. Clockwise from top left: streamline, pressure, ε and k

Table I. Flow separation details; γ is the detachment angle and L_r is the recirculation length, as shown in Figure 1

Model	γ	L_r
Linear k–ε	78°	4·02
Non-linear k–ε	79°	4·08
RNG k–ε	67°	3·63

4.6. *Comparison of results with experiment and between models*

Flow separation. The position of the detachment point 'd' is specified by the angle γ as shown in Figure 1. The recirculation length L_r is defined as the vertical distance between the centre of the inside bend (the semicircle) and the reattachment point 'r', also defined in Figure 1. Table I compares the flow separation details predicted by the three k–ε models. The shortest recirculation was predicted by the RNG model. The difference between the linear and non-linear k–ε models is very small in terms of separation details. It is interesting to note that a longer recirculation appears to be associated with a later detachment position (larger angle γ). Unfortunately, there are no experimental data on flow separation available for a detailed comparison.

As pointed out earlier, the non-linear k–ε model bears a certain resemblance to the Rivlin–Ericksen second-order model of viscoelastic flow. It is very interesting to note that there is very little difference in predicted velocity fields between the linear and non-linear k–ε models, despite the fact that the non-linear k–ε model yields quite complicated extra turbulent stresses as defined in (31). This seems to be analogous to the effect of second-order viscoelastic fluid models on laminar flow. In the case of laminar flow it has been proved[41] that under certain conditions the velocity field predicted by the second-order viscoelastic model remains *exactly* the same as that of a Newtonian flow and the non-linearities in the constitutive equations affect only the distribution of normal stress and pressure. However, for the classical problem of turbulent flow over a backward-facing step, Speziale and co-workers found[21,25,26] that the non-linear k–ε model predicted a longer recirculation length than the linear model and this was confirmed by our own calculations—our code predicted the recirculation length to be 6·35 for the linear and 6·56 for the non-linear k–ε model using van Driest mixing length wall functions.

Pressure distribution. Experimental data of pressure distributions on both internal and external walls were provided by Daimler Benz.[42] The normalized pressure coefficient is defined as

$$C_p = \frac{p - p_\infty}{\rho u_{in}^2/2}, \tag{46}$$

where p_∞ is the pressure at the entrance to the bend. The pressure data are measured as a function of dimensionless arc length s, starting and ending at the following points (normalization constant $s_0 = 9$ cm).

On the inside wall: $s = 0$ at 7·4 cm behind the inflow plane and $s = 1$ at 7·4 cm before the outflow plane. With this definition of s, the value of s at the beginning of the inside wall bend (the semicircle) is 0·393 and it is 0·606 at the end of the semicircle, which means that the detachment points of flow separation shown in Table I are located at about $s = 0{\cdot}5$.

On the outside wall: $s = 0$ at the starting point of the rigid wall on the symmetry axis (point A in Figure 1) and $s = 1{\cdot}320110$ at 9·54 cm before the outflow plane.

Figure 6 shows the outside wall pressure distribution curves predicted by the three k–ε models in the present study together with the experimental data. For a comparison, FIDAP's predictions[29] at experimental points are also plotted. As seen in Figure 6, unlike the situation of the velocity field,

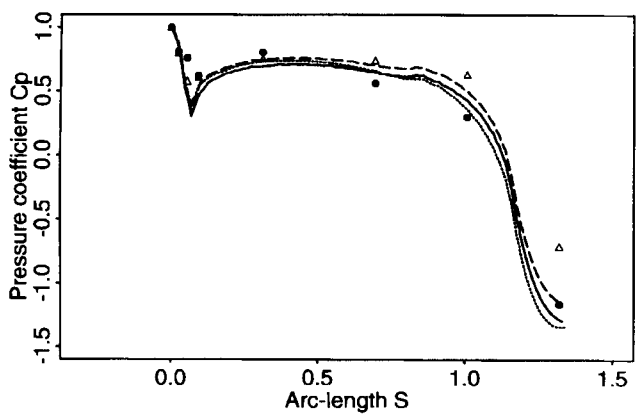

Figure 6. Outside wall pressure coefficient as a function of normalized arc length: - - -, linear k–ε model; —, non-linear k–ε model; . . . , RNG model; •, experiment;[42] △, FIDAP[29]

the difference in pressure distributions between the linear and non-linear k–ε models is much more pronounced as expected. On the whole the agreement of our predictions with experiment is good and the RNG and non-linear models gave slightly better predictions than the standard linear k–ε model.

The comparison of pressure data on the inside wall presented in Figure 7 shows a large discrepancy between all numerical predictions and experiment in the high-pressure-gradient region near the beginning of the inside bend (see also the pressure contours), with a large negative pressure peak in all numerical results. This large discrepancy indicates the need for better models or wall treatment in these kind of situations where no universal wall functions exist. Among the four predictions, the RNG model, which uses uniform viscosity expression, has the least discrepancy with experiment in the pressure peak region. Since experimental measurements were made only at a few points, much coarser than the computational nodes, the question as to whether the experimental points simply missed the negative pressure peak region remains to be answered. However, in any case the numerically predicted negative pressure peak seemed to be at least too wide, and the magnitude possibly too large, judging from the available limited number of experimental points.

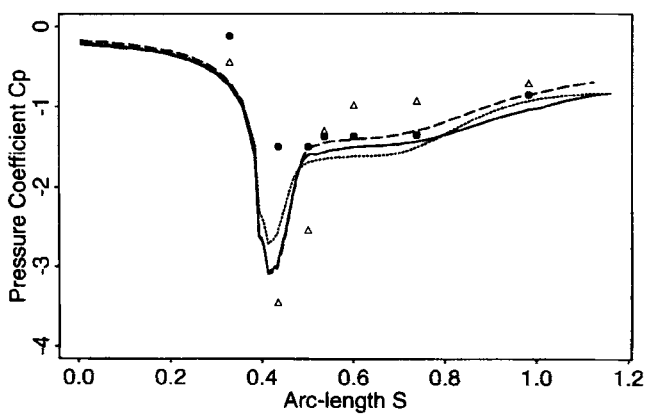

Figure 7. Inside wall pressure coefficient as a function of normalized arc length: - - -, linear k–ε model; —, non-linear k–ε model; . . . , RNG model; •, experiment;[42] △, FIDAP[29]

Apart from the negative pressure peak region, the agreement between our predictions and experiment on the inside wall is satisfactory. Unlike the situation on the outside wall, on the inside wall the RNG and non-linear k–ε models did not seem to do any better than the standard linear k–ε model, which may be attributed to the fact that the dominant influence on the inside wall is the high pressure gradient normal to the wall and all models failed there. The effect of a high pressure gradient on the outside wall is much less than on the inside wall, as is evident from all pressure contour plots in Figures 3–5.

Comparing pressure distributions between the linear and non-linear k–ε models in Figure 7, one notices there is little difference before $s = 0{\cdot}5$, which is about where the flow separation starts. Before the separation the flow is basically a fully developed shear flow and the normal stress difference predicted by the non-linear k–ε model does not affect the pressure distribution, similar to the situation of non-Newtonian laminar shear flow where a second-order fluid model predicts a non-zero normal stress difference but does not affect the pressure distribution. Downstream close to the outlet, the flow recovers to become a fully developed shear flow again and the pressure distribution curves predicted by the linear and non-linear models become parallel to each other, which shows that there is little non-linear effect on the pressure distribution (or the pressure gradient) downstream, the same as upstream before the flow separation.

5. CONCLUSIONS

A robust operator-splitting time-stepping algorithm for steady or transient turbulent flow has been implemented with finite elements using the unique *Fasttalk* language. Linear, non-linear and RNG-based k–ε models have been incorporated into the segregated time-stepping scheme.

The WUA-CFD benchmark problem of turbulent flow in an axisymmetric narrowing bend is solved with the three k–ε models and two different sets of wall functions. Calculations show that the operator-splitting time-stepping algorithm is very efficient, robust and stable. The usual problem of negative values of k and ε can be either completely avoided or minimized in the semi-implicit time-stepping scheme by limiting the magnitude of time steps.

The RNG model predicted flow separation without any difficulty; the linear and non-linear k–ε models failed to predict separation with a logarithmic profile one-layer wall function but succeeded with the van Driest mixing length wall function. This gives a clear explanation of why some reports at WUA-CFD '94 concluded that standard k–ε does not predict separation while others at the same meeting reached the opposite conclusion. Different groups at WUA-CFD '94 used different wall functions, but the present work has demonstrated that, with everything else the same, different wall functions can make the difference between complete failure and success in predicting flow separation for the WUA-CFD benchmark problem.

There is very little difference between the linear and non-linear k–ε models in terms of predicted velocity fields and the difference in predicted distributions of turbulent normal stress and pressure is much more pronounced, in analogy to the effect of second-order viscoelastic fluid models on laminar flow.

The comparison of predictions with experimental data on pressure distribution on solid walls shows good overall agreement, except in the high-pressure-gradient (normal to the wall) region near the detachment point on the inside wall. The large discrepancy between all predictions and experiment in the high-pressure-gradient near-wall region highlights once again the failure of using universal wall functions in non-universal flow regions and the need for better wall treatment in general.

Further work needed is to explore the use of better near-wall models,[15] low-Reynolds-number modifications[19] and other considerations such as the effect of curvature.[43–45]

ACKNOWLEDGEMENTS

This work is part of the *Fastflo* project, which is managed by a syndicate of CSIRO, Compumod and BHP and financially supported by the Department of Science, Industry and Technology of the Australian Government. The author wishes to thank Dr. Chin-Hsien Li for introducing him to operator-splitting techniques, Dr. Nick Stokes for helping with the usage of *Fasttalk* and Dr. Noel Barton for suggesting the bend problem.

REFERENCES

1. A. G. Hutton, R. M. Smith and S. Hickmott, 'The computation of turbulent flows of industrial complexity by the finite element method—progress and prospects', *Int. j. numer. methods fluids*, **7**, 1277–1298 (1987).
2. M. O. Bristeau, R. Glowinski, A. Hauguel and J. Periaux (eds., *Proc. Sixth Int. Symp. on Finite Element Methods in Flow Problems*, INRIA, 1986.
3. A. J. Baker and J. A. Orzechowski, 'An interaction algorithm for three-dimensional turbulent subsonic aerodynamic juncture region flow', *AIAA J.*, **21**, 524–533 (1983).
4. R. M. Smith, 'On the finite-element calculation of turbulent flow using the k–ε model', *Int. j. numer. methods fluids*, **4**, 303–319 (1984).
5. C. Taylor, C. E. Thomas and K. Morgan, 'Modelling flow over a backward-facing step using the FEM and the two-equation model of turbulence', *Int. j. numer. methods fluids*, **1**, 295–304 (1981).
6. P. L. Betts and V. Haroutunian, 'k–ε modelling of turbulent flow over a backward facing step by a finite element method, comparison with finite volume solutions and experiment', in C. Taylor, M. D. Olson, P. M. Gresho and W. G. Habashi (eds), *Numerical Methods in Laminar and Turbulent Flow*, Pineridge, Swansea, 1985.
7. J. Goussebaile, A. Jacomy, A. Hauguel and J. P. Gregoire, 'A finite element algorithm for turbulent flow processing a k–ε model', in C. Taylor, M. D. Olson, P. M. Gresho and W. G. Habashi (eds), *Numerical Methods in Laminar and Turbulent Flow*, Pineridge, Swansea, 1985.
8. B. Cardot, B. Mohammadi and O. Pironneau, 'A few tools for the implementation of turbulence models in Navier–Stokes solvers', in M. D. Gunzburger and R. a. Nicolaides (eds), *Incompressible CFD—Trends and Advances*, Cambridge University Press, Cambridge, 1991.
9. B. Mohammadi, 'Complex turbulent compressible flow computation using a two-layer approach', *Int. j. numer. methods fluids*, **15**, 747–771 (1992).
10. M. S. Engelman, *FIDAP Theoretical Manual—Version 7.0*, Fluid Dynamics International, 1993.
11. E. R. van Driest, 'On turbulent flow near a wall', *J. Aeronaut. Sci.*, **23**, 1007–1011 (1956).
12. W. P. Jones and B. E. Launder, 'The prediction of laminarization with a two-equation model of turbulence', *Int. Heat Mass Transfer*, **15**, 301 (1972).
13. K. Hanjalic and B. E. Launder, *J. Fluid Mech.*, **52**, 609 (1972).
14. B. E. Launder and D. B. Spalding, 'The numerical computation of turbulent flows', *Comput. Methods Appl. Mech. Eng.*, **3**, 269–289 (1974).
15. V. C. Patel, W. Rodi and G. Scheurer, 'Turbulence models for near-wall and low Reynolds number flows: a review', *AIAA J.*, **23**, 1308–1319 (1985).
16. V. Yakhot and S. and S. A. Orszag, 'Renormalization group analysis of turbulence: 1. Basic theory', *J. Sci. Comput.*, **1**, (1986).
17. V. Yakhot, S. A. Orszag, S. Thangam, T. B. Gatski and C. G. Speziale, 'Development of turbulence models for shear flows by a double expansion technique', *Phys. Fluids A*, **4**, 1510 (1992).
18. V. Yakhot and L. M. Smith, 'The renormalization group, the ε expansion and derivation of turbulence models', *J. Sci. Comput.*, **3**, 35 (1992).
19. S. A. Orszag, V. Yakhot, W. S. Flannery and F. Boysan, 'Renormalization group modelling and turbulence simulations', R. M. C. So and C. G. Speziale (eds), *Near Wall Turbulent Flows*, Elsevier, Amsterdam, 1993.
20. W. Rodi, 'Example of turbulence models for incompressible flows', *AIAA J.*, **20**, 872 (1982).
21. C. G. Speziale, 'On nonlinear k–l and k–ε models of turbulence', *J. Fluid Mech.*, **178**, 459–475 (1986).
22. C. Truesdell and W. Noll, 'The nonlinear field theories of mechanics', *Handb. Phys.*, **III/3**, (1965).
23. R. S. Rivlin, 'The relation between the flow of non-Newtonian fluids and turbulent Newtonian fluids', *Q. Appl. Maths.*, **15**, 212 (1957).
24. C. G. Speziale, 'On the origin of turbulent secondary flows in non-circular ducts', in *Computation of Internal Flows: Methods and Applications, ASME FED 14*, ASME, New York, 1984, p. 101.
25. C. G. Speziale and T. Ngo, 'Numerical solution of turbulent flow past a backward facing step using a nonlinear k–ε model', *Int. J. Eng. Sci.*, **26**, 1099–1112 (1988).
26. S. Thangam and N. Hur, 'A highly-resolved numerical study of turbulent separated flow past a backward-facing step', *Int. J. Eng. Sci.*, **29**, 607–615 (1991).
27. I. P. Jones and C. B. Hope, 'Axi-symmetric isothermal turbulent flow in a narrowing bend', *Report to WUA-CFD annual meeting*, Basel, 1994.

28. D. Choudhury, M. Rossi, D. LaRoche and F. Boysan, 'Solutions of the 1994 WUA-CFD test Problems using FLUENT', *Report to WUA-CFD annual meeting*, Basel, 1994.
29. M. Engelman, 'Axi-symmetric isothermal turbulent flow in a narrowing bend', *Report to WUA-CFD annual meeting*, Basel, 1994.
30. D. G. Lilley and D. L. Rhode, 'A computer code for swirling turbulent axisymmetric recirculating flows in practical isothermal combustor geometries', *NASA Contractor Rep. CR-3442*, 1982.
31. A. D. Gosman and F. J. K. Ideriah, 'TEACH-T: a general computer program for two-dimensional, turbulent recirculating flows', *Fluids Section Rep.*, Mechanical Engineering Department, Imperial College, London, 1976.
32. R. K. Boyd and J. H. Kent, 'Three-dimensional furnace computer modelling', *Proc. 21st Symp. (Int.) on Combustion*, Combustion Institute, London, 1986, pp. 265–274.
33. M. O. Bristeau, R. Glowinski and J. Periaux, *Comput. Phys. Rep.*, **6**, 73–187.
34. E. Dean, R. Glowinski and C. H. Li, 'Application of operator splitting methods to the numerical solution of nonlinear problems in continuum mechanics and physics', in J. Goldstein, S. Rosecrans and G. Sod (eds), *Mathematics Applied to Science*, 1988.
35. E. Dean, R. Glowinski and C. H. Li, 'Supercomputer solutions of partial differential equation problems in computational fluid dynamics and in control', *Comput. Phys. Commun.*, **53**, 401–439 (1989).
36. R. Glowinski and O. Pironneau, 'Finite element method for Navier–Stokes equations', *Ann. Rev. Fluid MEch.*, **24**, 167–204 (1992).
37. N. Stokes, *Fastflo Version 2.2, Fasttalk Manual*, CSIRO Division of Mathematics and Statistics, North Ryde, 1995 (more information available from WWW site: http://www.mel.dms.CSIRO.AU/nick/world/CC05.html).
38. *WUA-CFD Test Case 1/93*, Daimler Benz AG., Stuttgart, 1994.
39. F. Ginter, M. Heitele and A. Ruprecht, 'WUA-CFD Benchmark 1/93 results', *Report to WUA-CFD annual meeting*, Basel, 1994.
40. M. Schafer and N. Stosic, 'Results for WUA-CFD Test Case 1/93', *Report to WUA-CFD annual meeting*, Basel, 1994.
41. R. I. Tanner and A. C. Pipkin, *Trans. Soc. Rheol.*, **13**, 471 (1969).
42. *WUA-CFD Test Case 1/93 Experimental Data*, Daimler Benz AG., Stuttgart, 1994.
43. M. A. Leschziner and W. Rodi, 'Calculation of annular and twin parallel jets using various discretization schemes and turbulence model variations', *J. Fluids Eng.* **103**, 352–360 (1981).
44. F. Pourahmadi and A. C. Humphry, 'Predition of curved channel flow with an extended k–ε model of turbulence', *AIAA J.*, **21**, 1365–1373 (1983).
45. G. C. Chen and S. Farokhi, 'On turbulent flows dominated by curvature effects', *J. Fluids Eng.*, **114**, 52–57 (1992).